LAWRENCE
LIVERMORE
NATIONAL
LABORATORY

UCRL-JRNL-207566

Optical pump-probe processes in Nd 3+ doped KPb2Br5, RbPb2Br5, and KPb2CI5

K. Rademaker, G. Huber, S. A. Payne, E. Osiac, L. I. Isaenko

October 29, 2004

Journal of Optical Society of America B

Optical pump–probe processes in Nd^{3+} doped KPb_2Br_5, $RbPb_2Br_5$, and KPb_2Cl_5

Katja Rademaker [1), 2)], Guenter Huber [2)], Stephen A. Payne [1)],

Eugen Osiac[2)], Ludmila I. Isaenko[3)]

[1)] Lawrence Livermore National Laboratory, University of California, Livermore, California 94550, USA

[2)] Institut fuer Laser-Physik, Universitaet Hamburg, Luruper Chaussee 149, 22761 Hamburg, Germany

[3)] Design and Technological Institute for Monocrystals, Siberian Branch, Russian Academy of Sciences, 43 Russkaya, Novosibirsk 63005, Russia

Recently, laser activity has been achieved in the low phonon energy, moisture-resistant bromide host crystals, neodymium-doped potassium lead bromide (Nd^{3+}:KPb_2Br_5) and rubidium lead bromide (Nd^{3+}:$RbPb_2Br_5$).[1] Laser activity at 1.07 μm was observed for both crystalline materials. Laser operation at the new wavelengths 1.18 μm and 0.97 μm resulting from the $^4F_{5/2}+^2H_{9/2}\rightarrow{}^4I_J$ transitions (J=13/2 and 11/2) in Nd:RPB was achieved for the first time in a solid state laser material. In this paper we present cw pump-probe spectra in order to discuss excited state absorption, reabsorption processes due to the long lived lower laser levels as well as possible depopulation mechanisms feasible for more efficient laser operation in these crystals. The bromides will be compared with potassium lead chloride (Nd^{3+}:KPb_2Cl_5).

OCIS codes: (160.5690) Rare earth doped materials; (140.3380) Laser materials

I. INTRODUCTION

Recently, laser activity has been achieved for the first time in low phonon energy, moisture-resistant bromide host crystals: neodymium-doped potassium lead bromide (Nd^{3+}:KPb_2Br_5, KPB) and rubidium lead bromide (Nd^{3+}:$RbPb_2Br_5$, RPB).[1]

With a maximum peak value of ~ 138 cm^{-1} (KPB) and ~ 141 cm^{-1} (RPB)[2,3] the phonon energy in these materials is ~ 1.5 times smaller than in KPC (203 cm^{-1})[4] because of the higher atomic mass of the vibrating bromine constituents. This minimizes the nonradiative decay due to multiphonon interactions, in principle permitting lasing in the long wavelength region (e.g. 10 μm with dopant ions like Tb^{3+}).[2] In this paper we focus on the bromide hosts doped with the rare earth ion neodymium. In our previous studies[2,3] we revealed high emission rates of transitions originating from the $^4F_{5/2}$+ $^2H_{9/2}$ level relative to the $^4F_{3/2}$ level (Fig. 1) which demonstrates the greatly reduced nonradiative multiphonon decay rate of the bromide versus the chloride[4] (arising from the lower phonon energies). Laser activity at the new wavelength 1.18 μm arising from the $^4F_{5/2}$+$^2H_{9/2}$→$^4I_{13/2}$ transition in Nd:RPB was achieved for the first time in a solid state material (Fig. 2 adapted from Ref. 1). In the same crystal, laser activity at the wavelength 0.97 μm resulting from the $^4F_{5/2}$+$^2H_{9/2}$→$^4I_{11/2}$ transition was also demonstrated for the first time.[1] In both cases the upper laser level was pumped directly at 0.81 μm. Laser operation at 1.07 μm was also reported by pumping into the $^4F_{3/2}$ level of the neodymium doped MPB (M=Rb, K) crystals. The main purpose of the present study is to gain further insights into the lasing potential of Nd^{3+} in RPB and KPB.

In this paper we present cw pump-probe spectra in order to discuss excited state absorption (ESA) and reabsorption processes (RA) due to the long lived lower laser levels, as well as possible depopulation mechanisms feasible for more efficient laser operation in these bromide crystals. Oscillator strengths and effective cross sections of ESA and RA transitions competing with the (laser) emission transitions, as well as cross relaxation (CR) processes

among the lower laser levels, will be given. Figure 1 depicts the transitions responsible for the ESA, RA, CR, pump, and gain. For comparison pump-probe spectra will also be presented for the potassium lead chloride host (Nd^{3+}:KPb_2Cl_5).

II. EXPERIMENTAL SETUP

Excited state absorption spectra for the Nd doped bromide and chloride crystals are determined by a pump and probe method using the setup in Fig. 3. The technique described in the following was previously used to study e.g. Nd^{3+} doped oxides and fluorides like $Y_3Al_5O_{12}$, $YAlO_3$, Y_2O_3, YVO_4, $GdVO_4$, $Sr_5(PO_4)_3F$, $LaSc_3(BO_3)_4$, $CaWO_4$, $YLiF_4$, etc.[5-7] An unpolarized halogen lamp was used as the probe source while a cw Ti:Sapphire laser tuned to 0.75 μm, 0.81 μm and 0.89 μm pumped the $^4F_{7/2}$+$^4S_{3/2}$, $^4F_{5/2}$+$^2H_{9/2}$, and $^4F_{3/2}$ levels, respectively. The crystals were placed behind a 500 μm diameter pinhole, to ensure good overlap between pump and probe beam. The transmitted intensity was detected by using a liquid nitrogen cooled InSb-detector and a ½ m, 1μm blazed grating (600 l/mm) monochromator. In the double modulation technique described in detail in Koetke et al.[8] two lock-in amplifiers were used. The first lock-in amplifier detected the probe signal I_u modulated by a high frequency chopper (~ 1 kHz). The second lock-in amplifier isolates and amplifies the signal difference I_p-I_u of the pumped and unpumped signal intensity using a low frequency chopper (~ 10-15 Hz) to modulate the pump beam. The difference of the pumped and unpumped signal intensity I_p-I_u as well as the transmitted signal intensity I_u in absence of the pump beam are detected simultaneously.

The following equation illustrates the relation between the measured signal intensities and the competing ground state absorption (GSA), stimulated emission (em), excited state absorption (ESA) and reabsorption (RA) processes as shown for $I_p \approx I_u$ (valid in the case of small pump power densities meaning when the number of excited ions is small compared to the ground state density in the crystal):[8]

$$\frac{I_p - I_u}{I_u} = C \cdot n_e \cdot l \cdot [\sigma_{GSA} + \sum_i \frac{n_i}{n_e}(\sigma_{em,i} - \sigma_{ESA/RA,i})] \qquad [1]$$

where C is a constant, σ_{em}, $\sigma_{ESA,RA}$, σ_{GSA} are the cross sections, *l* the transmission path length, n_i is the population density of level i, and $n_e = \Sigma n_i$ the total excitation density summarized over all excited levels i. When ESA and/or reabsorption processes predominate the measured signal is negative while the signal is positive due to bleaching and/or stimulated emission. In our study the determination of ESA cross sections appeared to be difficult due to the fact that more than one metastable level is significantly populated in these materials. Here, the upper laser levels such as the $^4F_{3/2}$ and $^4F_{5/2}+^2H_{9/2}$ levels, as well as the lower long lived laser levels ^4I_J (J= e.g. 11/2, 13/2), contribute to the relevant population densities. Reabsorption competing with stimulated emission and/or ground state absorption taking part in the same wavelength region makes it difficult to establish an accurate value for the ESA cross section. Thus, we present a more qualitative discussion of the spectra and calculated effective cross sections by using the calculated transition strengths as explained in section III. Emission measurements were performed by using the same monochromator-detector system and excitation source as described above.

III. SPECTROSCOPIC RESULTS AND DISCUSSION

Cw pump-probe spectra were determined for Nd:KPB, Nd:RPB and Nd:KPC ranging from 780 – 1550 nm by pumping into the $^4F_{3/2}$, $^4F_{5/2}+^2H_{9/2}$ and $^4F_{7/2}+^4S_{3/2}$ levels, respectively. Note that emission (thick line) and pump-probe spectra (thin line) in Figure 4 and 5 - displayed on different scales - can not be compared quantitatively. In order to simplify this discussion, potential transitions resulting from the $^4F_{7/2}+^4S_{3/2}$ level (Fig. 1) have been neglected in this study, assuming that the relaxation between the $^4F_{7/2}+^4S_{3/2}$ and $^4F_{5/2}+^2H_{9/2}$ levels is fast. Future studies on transitions resulting from the $^4F_{7/2}+^4S_{3/2}$ level may be interesting in order to

determine the emission and ESA properties (as relatively strong signal strengths for these transitions have been calculated).

Figure 4 shows the measured spectra of a Nd:KPB crystal in the wavelength region 780-1500 nm. The spectra are determined by pumping into the $^4F_{3/2}$ (a) and $^4F_{7/2}$+$^4S_{3/2}$ (b) levels, shown in the upper and lower frames, respectively. The inset in (b) displays a magnification for the peaks in the wavelength range 1135 – 1500 nm. Spectra measured by pumping into the $^4F_{5/2}$+$^2H_{9/2}$ level showed in principle similar features to the spectrum shown in Fig. 4(b). Reabsorption and excited state absorption compete with gain as indicated.

The pump-probe spectra in Figure 4 show reabsorption features resulting from the $^4I_{11/2}$ and $^4I_{13/2}$ levels as indicated. The peak RA wavelength matches the peak wavelength in emission as expected. The ratio of reabsorption transitions emanating from the $^4I_{13/2}$ and $^4I_{11/2}$ levels proves that the $^4I_{13/2}$ population is reduced compared to the $^4I_{11/2}$ level population, which is likely due to cross relaxation (CR, see Fig.1) and/or radiative processes. The influence of multiphonon decay is small because of the large energy gap to the next lowest level ~2000 cm^{-1} involving more than 14 phonons.

The calculated transitions, their signal strengths, and their effective cross sections are listed in Table 1(a). The line strengths S of induced electric dipole (ED) transitions are calculated by using the Judd-Ofelt intensity parameters[9,10] Ω_2= 15.70, Ω_4= 6.25, Ω_6= 2.96 [10^{-20} cm^2] of Nd:KPB and the reduced matrix elements given in Kaminskii.[2,11] The line strengths S of magnetic dipole (MD) transitions were calculated in the intermediate coupling scheme by using the formulas given in Weber[12] for calculating S^{MD} in the LS coupling scheme and by using the energy eigenvectors of intermediate coupled states for Nd^{3+} from Wybourne[13]. The effective cross sections are calculated by using the following formula:

$$\Sigma^{eff} = \frac{\int \sigma d\lambda}{\overline{\lambda}^2} = \frac{4\pi^2 e^2}{3\hbar c} \cdot \frac{1}{\overline{\lambda} \cdot (2J+1)} \left[\frac{(n^2+2)^2}{9n} S^{ED} + nS^{MD} \right] = \frac{A_{JJ'} \cdot \overline{\lambda}^2}{8\pi c n^2}, \quad [2]$$

where J is the initial level, n the averaged refractive index (2.16 for KPB, 2.08 for RPB)[2], S^{MD} and S^{ED} the calculated signal strengths of magnetic dipole and induced electric dipole, $A_{JJ'}$ the spontaneous emission rates[14], and $\bar{\lambda}$ is the averaged wavelength of the transition (calculated by taking the difference of the centroids of the crystal field levels of Nd:KPB). Table 2 shows the calculated radiative lifetimes and measured lifetimes for relevant initial levels in neodymium-doped KPB, RPB and KPC discussed in this study. The radiative lifetime of the $^4I_{11/2}$ level in Nd:KPB is calculated to be about 3-4 times longer than for the other ^4I_J levels (J=13/2, 15/2). The branching ratio of the $^4F_{5/2}+{}^2H_{9/2} \rightarrow {}^4I_{13/2}$ transition is calculated to be similar as revealed by emission spectrum[2] and higher as revealed from Judd-Ofelt[2], to the branching ratio of the $^4F_{5/2}+{}^2H_{9/2} \rightarrow {}^4I_{11/2}$ transition in Nd:KPB. The Nd:KPB transitions of Table 1(a) thought to be observed as the main transitions in the spectra of Fig. 4 are denoted with an asterisk. Table 1(b) contains the results for Nd:RPB, to be discussed below.

Interestingly, due to the following discussion of the cw pump-probe spectra from the crystals Nd:KPB, Nd:RPB and Nd:KPC with different Nd dopant concentrations, we suggest that the $^4I_{13/2}$ depopulation occurs via cross relaxation (Fig. 1, Tab. 3) leading mainly to less reabsorption of transitions from the $^4I_{13/2}$ level compared to the $^4I_{11/2}$; as a result, the $^4F_{5/2}+{}^2H_{9/2} \rightarrow {}^4I_{13/2}$ transition is more favorable for efficient laser operation at 1.18 μm for longer pulses or even cw pumping. Referring to Fig. 4, we see that net gain is observed for this transition of high cross section at 1.18 μm in contrast to reabsorption at 1.07 μm and at 0.97 μm due to the shorter level lifetime of the $^4I_{13/2}$ versus $^4I_{11/2}$. Of course, laser action was observed for all of these transitions (1.18 μm, 0.97 μm and 1.07 μm)[1] as shown for two of these wavelengths in Fig. 2 due to the short pump pulse length (~10 ns). Following a study in Nd:KPC[15], cross relaxation is significant for Nd concentrations $\geq 2(\pm1)\cdot10^{19}$ cm^{-3}. This is revealed by fitting the lifetime data of Nd:KPC in Ref. 15 to $\tau=\tau_0/(1+(c/c_0)^2)$ where c stands

for the concentration and c_0, and τ_0 are parameters. In Nd:KPC the lifetime of the $^4I_{13/2}$ level is reported to drop from 6 ms to 0.3 ms if the concentration is increased from $0.88 \cdot 10^{19}$ cm^{-3} to $7.4 \cdot 10^{19}$ cm^{-3}.[15] The Nd:KPB sample used in our measurements has a Nd concentration N_c of $\sim 4 \cdot 10^{19}$ cm^{-3}, suggesting fast cross relaxation occurs. As shown later in this section no net gain is observed at 1.18 μm for either the Nd:KPC crystal (due to fast relaxation out of the $^4F_{5/2}+^2H_{9/2}$ level (2 μs, Tab. 2)), nor for the Nd:RPB crystal (due to low Nd concentration and absence of significant cross relaxation), compare Figures 4 and 5. Reabsorptions resulting from the $^4I_{15/2}$ level are also weak e.g. due to cross relaxation processes as indicated in Figure 1 and Table 3 (measurements show e.g. that the $^4I_{15/2} \rightarrow {}^4I_{11/2}$ emission overlaps the $^4I_{9/2} \rightarrow {}^4I_{13/2}$ absorption transition[16]).

As noted, the use of different pump wavelengths have a significant impact on the spectra. While pumping into the $^4F_{3/2}$ level (Fig. 4(a)) shows reabsorption e.g. at 1.18 μm, gain is observed at 1.18 μm by pumping into the $^4F_{7/2}+{}^4S_{3/2}$ level (Fig. 4(b)). In addition, excited state absorption at ~1.45 μm resulting from the $^4F_{5/2}+{}^2H_{9/2}$ level into the $^4G_{9/2}$ is observed only if the $^4F_{5/2}+{}^2H_{9/2}$ level is populated Fig. 4(b)). In contrast, excited state absorption from the $^4F_{3/2}$ level into the $^4G_{9/2}$ is observed at ~1.26 μm only by pumping the $^4F_{3/2}$ level directly (Fig. 4(b)). Excited state absorption from the $^4F_{3/2}$ level into the $^4G_{7/2}$ at ~1.33 μm as well as gain resulting from the $^4F_{3/2} \rightarrow {}^4I_{13/2}$ transition at ~1.35 μm is observed if the $^4I_{13/2}$ level is rapidly depopulated by cross relaxation and the $^4F_{3/2}$ level is directly pumped (Fig. 4(a)). Note, that the gain of the $^4F_{5/2}+^2H_{9/2} \rightarrow {}^4I_{13/2}$ is bigger than for $^4F_{3/2} \rightarrow {}^4I_{13/2}$ (Fig. 4(b)) since the $^4F_{7/2}+{}^4S_{3/2}$ level is pumped, and the cross section of the transition resulting from the combined $^4F_{5/2}+^2H_{9/2}$ level into the $^4I_{13/2}$ level is slightly higher than for the $^4F_{3/2} \rightarrow {}^4I_{13/2}$ transition. Also, the above mentioned influence of ESA observed for the $^4F_{3/2} \rightarrow {}^4I_{13/2}$ transition defeats gain. We do not observe ESA influencing the $^4F_{5/2}+^2H_{9/2} \rightarrow {}^4I_{13/2}$ even though it is predicted (e.g. $^2H_{9/2} \rightarrow {}^2K_{15/2}$, Table 1).

The negative features around 0.79 and 0.88 μm are mainly due to reabsorption from the $^4I_{11/2} \rightarrow {}^4F_{9/2}$ and $^4I_{11/2} \rightarrow {}^4F_{7/2} + {}^4S_{3/2}$ transitions, respectively. The nearby positive features arise from bleaching of the ground state absorption and emission.

Other laser transitions and depopulation mechanisms might be considered. For example, the $^4F_{5/2} + {}^2H_{9/2} \rightarrow {}^4I_{15/2}$ transition at 1.56 μm (not shown; emission band in the wavelength range 1.47-1.65 μm[16]). Moreover, alternative depopulation mechanisms for the long-lived lower ^4I_J laser levels could involve the use of codopants with appropriate absorption lines such as Tb^{3+}; which has an absorption feature in the region ~ 4.2-5.6 μm and could depopulate e.g. the $^4I_{11/2}$ level.[2]

The pump-probe and emission spectra of a Nd:RPB crystal displayed in Fig. 5(b) are induced by pumping into the $^4F_{7/2} + {}^4S_{3/2}$ level. The transitions and their signal strengths are listed in Table 1(b). The line strengths S of induced electric dipole (ED) are calculated for Nd:KPB by using the Judd-Ofelt intensity parameters for Nd:RPB[2] $\Omega_2 = 0.41$, $\Omega_4 = 9.32$, $\Omega_6 = 2.56$ [10^{-20} cm^2]. The Nd:RPB crystal reveals similar features to Nd:KPB (Fig. 4(b)). The difference in the peak relation around 0.81 μm and 0.89 μm of Nd:KPB and Nd:RPB reflects e.g. higher absorption of the $^4I_{9/2} \rightarrow {}^4F_{5/2} + {}^2H_{9/2}$ versus the $^4I_{9/2} \rightarrow {}^4F_{3/2}$ transition in Nd:RPB.[2] The differences in the wavelength region 1150-1500 could possibly be explained by lower concentrations of Nd^{3+} in the sample used ($N_c \sim 6.3 \cdot 10^{18}$ $cm^{-3} << c_0$) leading to minimal cross relaxation and higher reabsorption from the $^4I_{13/2}$ level. Moreover, the signal strengths for the cross relaxation processes in Nd:RPB are calculated to be a little weaker than in Nd:KPB (Tab. 2). The oscillator strenghts for the ESA transitions at ~ 1.45 μm ($^4F_{5/2} + {}^2H_{9/2} \rightarrow {}^4G_{9/2}$) and 1.3 μm ($^4F_{3/2} \rightarrow {}^4G_{7/2}$) are weaker in Nd:RPB (Tab. 1(b)) than in Nd:KPB (Tab. 1(a)) while the oscillator strengths for reabsorption are similar.

The spectra of a Nd:KPC crystal displayed in Fig. 5(a) for the wavelength region 850-1500 nm are measured by pumping into the $^4F_{5/2} + {}^2H_{9/2}$ level. The Nd:KPC spectrum is comparable

with the pump-probe spectrum of Nd:KPB in Figure 4(a), where the $^4F_{3/2}$ level is directly pumped. This is the case because the $^4F_{3/2}$ level is rapidly populated following 0.81 μm pumping for Nd:KPC. The missing ESA transition at ~ 1.45 μm ($^4F_{5/2}+^2H_{9/2} \rightarrow ^4G_{9/2}$) in the chloride (in contrast to the bromide) can be explained by fast nonradiative decay from the $^4F_{5/2}+^2H_{9/2}$ level into the $^4F_{3/2}$ level (quantum efficiency ~ 0.013 for Nd:KPC due to the higher multiphonon decay rate).[2,4] The missing reabsorption features from the $^4I_{13/2}$ is probably due to the high concentration of Nd^{3+} in the sample used in the experiments ($N_c \sim 1.5 \cdot 10^{20}$ $cm^{-3} > c_0$) leading to enhanced cross relaxation and depopulation of this level. The ratio of the negative feature and positive feature around 0.89 μm seem to be different if compared with Nd:KPB and Nd:RPB indicating probably higher reabsorption from the $^4I_{11/2}$. Also, the ratio of the reabsorption from the $^4I_{11/2} \rightarrow ^4F_{3/2}$ versus $^4I_{11/2} \rightarrow ^4F_J$ (J=5/2 and 7/2) is reduced which could indicate that gain is competing more effectively against reabsorption at 1.07 μm in Nd:KPC. The positive signal at ~ 1.1 μm was not reproducible and we can not be certain that it is actually due to gain. The positive pump-probe feature at 1.35 μm is likely due to net $^4F_{3/2} \rightarrow ^4I_{13/2}$ gain, while the nearby negative band at 1.33 μm is the well-known $^4F_{3/2} \rightarrow ^4G_{7/2}$ ESA. Finally, the 1.26 μm $^4F_{3/2} \rightarrow ^4G_{9/2}$ band is observed, as was the case for direct pumping of the $^4F_{3/2}$ level for Nd:KPB.

IV. SUMMARY

Cw pump-probe spectra and emission spectra were determined for the laser crystals Nd:KPB, Nd:RPB and Nd:KPC ranging from 780 – 1550 nm by pumping into the $^4F_{3/2}$, $^4F_{5/2}+^2H_{9/2}$ and $^4F_{7/2}+^4S_{3/2}$ levels, respectively in order to gain further insights into the lasing potential of Nd^{3+} in these low phonon energy moisture resistant crystals. Pump-probe spectra are presented in order to discuss excited state absorption (ESA) and reabsorption processes (RA) due to the long lived lower laser levels, as well as $^4I_{13/2}$ depopulation mechanisms feasible for more

efficient cw laser operation (i.e. cross relaxation and energy transfer to additional dopants). Calculated and measured lifetimes of the bromides are compared with the chloride for the most important initial levels discussed in this study. Oscillator strengths and effective cross sections of ESA and RA transitions competing with the (laser) emission transitions, as well as cross relaxation (CR) processes among the lower laser levels, are given for the bromide crystals.

Net cw gain is observed at the laser wavelength 1.18 μm for Nd:KPB in contrast to the reabsorption features at the laser wavelengths 1.07 μm and at 0.97 μm. In contrast, no gain is observed at 1.18 μm for Nd:KPC (due to fast relaxation out of the $^4F_{5/2}+^2H_{9/2}$ level), nor for Nd:RPB (due to low Nd concentration and absence of significant cross relaxation). The investigation of crystals of different Nd dopant concentrations suggest that the $^4I_{13/2}$ lower laser level depopulation occurs via cross relaxation leading mainly to less reabsorption of transitions from the $^4I_{13/2}$ level compared to the $^4I_{11/2}$; as a result, the $^4F_{5/2}+^2H_{9/2} \rightarrow ^4I_{13/2}$ transition is more favorable for efficient laser operation at 1.18 μm for longer pulses or even cw pumping at high Nd concentration. In future studies gain measurements would be useful in order to explain the population dynamics and to study the influence of different rare earth ion concentrations on laser oscillation (regarding self-termination). Future work on emission from energy levels of different rare earth ions with even smaller gaps to the next lower level like $^4F_{7/2}+^4S_{3/2}$ in Nd^{3+} can be interesting.

V. ACKNOWLEDGMENTS

The authors would like to thank especially Stefan Kueck at the Physikalisch-Technische Bundesanstalt, and Dione F. deSousa at the University of Hamburg for their advice in the ESA measurements. We are also very thankful about the support from Ernst Heumann, Klaus Petermann, and Volker Peters at the University of Hamburg. We are very grateful to William F. Krupke (ret. LLNL) and Mike Nostrand (LLNL) concerning their help and guidance e.g. in

the Judd-Ofelt calculations. This work was performed under the auspices of the U.S. Department of Energy by the University of California, Lawrence Livermore National Laboratory under Contract No. W-7405-Eng-48.

VI. REFERENCES

[1] K. Rademaker, Ernst Heumann, S.A. Payne, G. Huber, W. F. Krupke, L.I. Isaenko, A. Burger, "Laser activity at 1.18 μm, 1.07 μm, and 0.97 μm in the low phonon energy hosts KPb_2Br_5 and $RbPb_2Br_5$ doped with Nd^{3+} ", submitted to Opt. Lett. (2004)

[2] K. Rademaker, W. F. Krupke, R. H. Page, S.A. Payne, K. Petermann, G. Huber, A.P. Yelisseyev, L.I. Isaenko, U.N. Roy, A. Burger, K.C. Mandal, K. Nitsch, "Optical properties of Nd^{3+} and Tb^{3+} doped KPb_2Br_5 and $RbPb_2Br_5$ with low nonradiative decay", J. Opt. Soc. Am. B **x**, in press (2004)

[3] K. Rademaker, K. Petermann, G. Huber, W. F. Krupke, R. H. Page, S.A. Payne, A.P. Yelisseyev, L.I. Isaenko, U.N. Roy, A. Burger, K.C. Mandal, K. Nitsch, "Slow nonradiative decay for rare earths in KPb_2Br_5 and $RbPb_2Br_5$", ASSP, Santa Fe, New Mexico, USA, 2004

[4] M.C. Nostrand, R.H. Page, and S.A. Payne, L.I. Isaenko, A.P. Yelisseyev, "Optical properties of Dy^{3+}- and Nd^{3+}-doped KPb_2Cl_5", J. Opt. Soc. Am. B **18**, no. 3, 264-276 (2001)

[5] S. Kueck, L. Fornasiero, E. Mix, G. Huber, "Excited state absorption and stimulated emission of Nd^{3+} in crystals. Part I: $Y_3Al_5O_{12}$, $YAlO_3$, and Y_2O_3", Appl. Phys. B **67**, 151-156 (1998)

[6] L. Fornasiero, S. Kueck, T. Jensen, G. Huber, B.H.T. Chai, "Excited state absorption and stiumlated emission of Nd^{3+} in crystals. Part II: YVO_4, $GdVO_4$, $Sr_5(PO_4)_3F$", Appl. Phys. B **67**, 549-553 (1998)

[7] L. Fornasiero, T. Kellner, S. Kueck, J.P. Meyn, P.E.-A. Moebert, G. Huber, "Excited state absorption and stimulated emission of Nd^{3+} in crystals III: $LaSc_3(BO_3)_4$, $CaWO_4$, $YLiF_4$", Appl. Phys. B **68**, 67-72 (1999)

[8] J. Koetke, G. Huber, "Infrared excited-state absorption and stimulated-emission cross sections of Er^{3+}-doped crystals", Appl. Phys. B **61**, 151-158 (1995)

[9] B.R. Judd, "Optical absorption intensities of rare-earth ions", Phys. Rev. **127**, 750-761 (1962)

[10] G.S. Ofelt, "Intensities of crystal spectra of rare-earth ions", J. Chem. Phys. **37**, 511-520 (1962)

[11] A.A. Kaminskii, "Crystalline Lasers: Physical Processes and Operating Schemes", CRC Press, New York (1996)

[12] M.J. Weber, "Probabilities for radiative and nonradiative Decay of Er^{3+} in LaF_3, Phys. Rev. **157**, no. 2, 262-272 (1967)

[13] B.G. Wybourne, "Composition of the electronic states of Nd(IV) and Er(IV)", J. Chem. Phys. 34, no.1, 279-281 (1961)

[14] A.A. Kaminskii, Laser crystals, Their Physics and Properties, Springer Verlag, Berlin Heidelberg New York (1990)

[15] N.W. Jenkins, S.R. Bowman, L.B. Shaw, J.R. Lindle, "Spectroscopic analysis and laser modelling of neodymium-doped potassium lead chloride", J. Lum. **97**, 127-134 (2002)

[16] unpublished results

[17] unpublished results from Mike Nostrand, Lawrence Livermore National Laboratory

[18] U. Hoemmerich, E. Nyein, S.B. Trivedi, "Crystal growth, upconversion, and emission properties of Er^{3+}-, and Nd^{3+}- doped KPb_2Br_5", CLEO, San Francisco, CA, USA (2004)

Inscription of the Tables:

Table 1(a). Calculated line strengths S of induced electric dipole (ED) and of magnetic dipole (MD) transitions for relevant emission (EM), reabsorption (RA), bleaching and excited state absorption (ESA) transitions for Nd:KPB. The electric dipole quantities are calculated with the following Judd-Ofelt parameters: Ω_2= 15.70, Ω_4= 6.25, Ω_6= 2.96 [x10^{-20} cm^2]. The magnetic dipole quantities are determined in the intermediate coupling scheme (values < 0.01 are not listed). The effective cross section Σ^{eff} is calculated by using Eqn. (2) in section III.

Table 1(b). Calculated line strengths S of induced electric dipole (ED) and of magnetic dipole (MD) transitions for relevant emission (EM), reabsorption (RA), bleaching and excited state absorption (ESA) transitions for Nd:RPB. The electric dipole quantities are calculated with the following Judd-Ofelt parameters: Ω_2= 0.41, Ω_4= 9.32, Ω_6= 2.56 [x10^{-20} cm^2]. The magnetic dipole quantities are determined in the intermediate coupling scheme (values < 0.01 are not listed). The effective cross section Σ^{eff} is calculated by using Eqn. (2) in section III.

Table 2. Calculated radiative τ^{rad} and measured τ^{meas} lifetimes for the initial level J of the relevant emission, reabsorption, cross relaxation, and excited state absorption processes for Nd:KPB and Nd:RPB. For comparison lifetimes of Nd:KPC are given.

Table 3. Calculated line strengths S of induced electric dipole (ED)

and of magnetic dipole (MD) transitions for Nd:KPB (a) and Nd:RPB (b). Cross relaxation (CR) depopulates the lower long lived laser levels ^4I_J (J=13/2 and 15/2). The integrated cross sections Σ^{eff} of Nd:KPB are slightly higher than for Nd:RPB.

Inscription of the Figures:

Fig. 1. Energy level diagram of Nd:MPB (M= K, Rb) displays new laser transitions from the $^4F_{5/2}$+ $^2H_{9/2}$ level at 1.18 and 0.97 μm and potential transitions at 0.82 and 1.55 μm, in addition to the conventional laser transitions at 1.07 and 1.35 μm from the $^4F_{3/2}$ level. Excited state absorption transitions resulting from the $^4F_{5/2}$+ $^2H_{9/2}$ and $^4F_{3/2}$ levels as well as depopulation mechansims for the long lived lower laser levels ^4I_J (J=13/2, 15/2) via cross relaxation (CR) are indicated. The pump bands at 0.75, 0.81, and 0.89 μm are indicated. (Transitions resulting from the $^4F_{7/2}$+ $^4S_{3/2}$ level have been neglected in order to simplify the discussion.)

Fig. 2. Input-output characteristic for an OPO-pumped Nd:KPB crystal lasing at 1.07 μm and Nd:RPB crystal lasing at 1.07 μm and 1.18 μm (taken from Ref. 1). The slope efficiency is given for output pulse energy with respect to absorbed pump energy. In order to achieve lasing at 1.07 μm the $^4F_{3/2}$ level was directly pumped, while for the laser wavelength 1.18 μm and 0.97 μm the $^4F_{5/2}$ level was pumped.

Fig. 3. Experimental setup of the cw pump-probe technique.

Fig. 4. Emission spectra (thick line) and pump-probe spectra (thin line) of Nd^{3+}:KPb_2Br_5 determined by pumping into either the $^4F_{3/2}$ (a) or $^4F_{7/2}$+$^4S_{3/2}$ (b) level, respectively (using same crystal for both spectra). The inset in (b) displays a ~ 5x magnification for the wavelength range 1135 – 1500 nm. Reabsorption and excited state absorption compete with gain as indicated. Depopulation via cross relaxation leads to less reabsorption of transitions

from the $^4I_{13/2}$ level compared to the $^4I_{11/2}$. Note that only the main transitions are indicated (Table 1 shows others) and that the $^4F_{5/2}$+$^2H_{9/2}$ and $^4F_{7/2}$+$^4S_{3/2}$ levels are abbreviated by $^4F_{5/2}$ and $^4F_{7/2}$, respectively.

Fig. 5. Emission spectra (thick line) and pump-probe spectra (thin line) of Nd^{3+}:KPb_2Cl_5 determined by pumping into the $^4F_{5/2}$+$^2H_{9/2}$ level (a) and Nd^{3+}:$RbPb_2Br_5$ determined by pumping into the $^4F_{7/2}$+$^4S_{3/2}$ level (b). Reabsorption and excited state absorption compete with gain as indicated. Depopulation via cross relaxation leads to less reabsorption of transitions from the $^4I_{13/2}$ level compared to the $^4I_{11/2}$ in the case of Nd:KPC compared to Nd:RPB, due to the higher Nd concentration. (Note the emission of Nd:RPB is not blackbody corrected.) The feature near 0.94 μm (b) could be due to the $^4I_{13/2}\rightarrow{}^4F_{9/2}$ transition. Note that only the main transitions are indicated (Table 1 shows others) and that the $^4F_{5/2}$+$^2H_{9/2}$ and $^4F_{7/2}$+$^4S_{3/2}$ levels are abbreviated by $^4F_{5/2}$ and $^4F_{7/2}$, respectively.

Table 1(a). Calculated line strengths S of induced electric dipole (ED) and of magnetic dipole (MD) transitions for relevant emission (EM), reabsorption (RA), bleaching and excited state absorption (ESA) transitions for Nd:KPB. The electric dipole quantities are calculated with the following Judd-Ofelt parameters: Ω_2= 15.70, Ω_4= 6.25, Ω_6= 2.96 [x10^{-20} cm^2]. The magnetic dipole quantities are determined in the intermediate coupling scheme (values < 0.01 are not listed). The effective cross section Σ^{eff} is calculated by using Eqn. (2) in section III.

λ (μm)	Emission Transition (J→J')	$S^{ED}+S^{MD}$ [x10^{-20}cm^2]	Σ^{eff} [x10^{-18}cm]	ESA/ Bleaching / Reabsorption Transitions (J→J')	$S^{ED}+S^{MD}$ [x10^{-20}cm^2]	Σ^{eff} [x10^{-18}cm]
1.44				$^4F_{5/2}\rightarrow{}^4G_{9/2}$*	3.79	9.61
1.48				$^2H_{9/2}\rightarrow{}^4G_{9/2}$*	1.17+0.01	1.74
1.36	$^4F_{3/2}\rightarrow{}^4I_{13/2}$*	0.62	2.49	$^4I_{13/2}\rightarrow{}^4F_{3/2}$*	0.62	0.71
1.37				$^4I_{15/2}\rightarrow{}^4F_{7/2}$	2.80	2.80
1.35				$^4I_{15/2}\rightarrow{}^4S_{3/2}$	0.98	0.99
1.34				$^4F_{3/2}\rightarrow{}^2K_{13/2}$	0.02	0.09
1.335				$^4F_{3/2}\rightarrow{}^4G_{7/2}$*	1.91	7.85
1.255				$^4F_{3/2}\rightarrow{}^4G_{9/2}$*	0.82	3.60
1.19	$^4F_{5/2}\rightarrow{}^4I_{13/2}$*	2.32	7.11	$^4I_{13/2}\rightarrow{}^4F_{5/2}$*	2.32	3.05
1.17	$^2H_{9/2}\rightarrow{}^4I_{13/2}$*	0.99	1.86	$^4I_{13/2}\rightarrow{}^2H_{9/2}$*	0.99	1.33
1.21				$^2H_{9/2}\rightarrow{}^2K_{15/2}$ [(a)]	4.21	7.65
1.18				$^4F_{5/2}\rightarrow{}^2K_{15/2}$	0.02	0.05
1.20				$^2H_{9/2}\rightarrow{}^2G_{9/2}$	0.46+0.04	0.92
1.17				$^4F_{5/2}\rightarrow{}^2G_{9/2}$	0.89	2.78
1.17				$^2H_{9/2}\rightarrow{}^2D_{3/2}$	0.44	0.83
1.15				$^4F_{5/2}\rightarrow{}^2D_{3/2}$	0.06+0.01	0.23
1.14				$^2H_{9/2}\rightarrow{}^4G_{11/2}$ [(a)]	2.75+0.01	5.31
1.12				$^4F_{5/2}\rightarrow{}^4G_{11/2}$ [(a)]	0.97	3.16
1.07	$^4F_{3/2}\rightarrow{}^4I_{11/2}$*	1.93	9.84	$^4I_{11/2}\rightarrow{}^4F_{3/2}$*	1.93	3.28
1.07				$^4I_{13/2}\rightarrow{}^4F_{7/2}$	2.05	3.00
1.06				$^4I_{13/2}\rightarrow{}^4S_{3/2}$	0.98	1.45
1.02				$^4I_{15/2}\rightarrow{}^2H_{11/2}$	2.49	3.36
1.05				$^4F_{3/2}\rightarrow{}^2K_{15/2}$	0.03	0.15
1.045				$^4F_{3/2}\rightarrow{}^2G_{9/2}$	0.20	1.04
1.00				$^4F_{3/2}\rightarrow{}^4G_{11/2}$	0.30	1.66
0.97	$^4F_{5/2}\rightarrow{}^4I_{11/2}$*	1.16	4.39	$^4I_{11/2}\rightarrow{}^4F_{5/2}$*	1.16	2.20

0.95	$^2H_{9/2}\rightarrow{}^4I_{11/2}$*	0.12	0.29	$^4I_{11/2}\rightarrow{}^2H_{9/2}$*	0.12	0.24
0.94				$^4I_{13/2}\rightarrow{}^4F_{9/2}$*	2.95	4.92
0.96				$^2H_{9/2}\rightarrow{}^2P_{1/2}$	0.55	1.26
0.94				$^4F_{5/2}\rightarrow{}^2P_{1/2}$	0.15	0.57
0.89	$^4F_{3/2}\rightarrow{}^4I_{9/2}$*	1.60	9.81	$^4I_{9/2}\rightarrow{}^4F_{3/2}$*	1.60	3.92
0.885				$^4I_{11/2}\rightarrow{}^4F_{7/2}$*	2.41	4.98
0.88				$^4I_{11/2}\rightarrow{}^4S_{3/2}$*	0.62	1.29
0.84				$^4I_{13/2}\rightarrow{}^2H_{11/2}$	0.19	0.36
0.91				$^2H_{9/2}\rightarrow{}^2D_{5/2}$	0.55	1.32
0.89				$^4F_{5/2}\rightarrow{}^2D_{5/2}$	0.15	0.60
0.86				$^4F_{3/2}\rightarrow{}^2P_{1/2}$	0.20	1.29
0.82	$^4F_{5/2}\rightarrow{}^4I_{9/2}$*	2.67	11.97	$^4I_{9/2}\rightarrow{}^4F_{5/2}$*	2.67	7.18
0.805	$^2H_{9/2}\rightarrow{}^4I_{9/2}$*	0.54+0.02	1.51	$^4I_{9/2}\rightarrow{}^2H_{9/2}$*	0.54+0.02	1.51
0.79				$^4I_{11/2}\rightarrow{}^4F_{9/2}$*	1.31	3.01
0.78				$^4I_{15/2}\rightarrow{}^2K_{13/2}$	0.03	0.05
0.81				$^4F_{3/2}\rightarrow{}^2D_{5/2}$	0.20	1.35

[(a)]Not clear why these transitions are not observed.
*Indicated as the main observed transitions for Nd:KPB in Figure 4.

Table 1(b). Calculated line strengths S of induced electric dipole (ED) and of magnetic dipole (MD) transitions for relevant emission (EM), reabsorption (RA), bleaching and excited state absorption (ESA) transitions for Nd:RPB. The electric dipole quantities are calculated with the following Judd-Ofelt parameters: Ω_2= 0.41, Ω_4= 9.32, Ω_6= 2.56 [x10^{-20} cm^2]. The magnetic dipole quantities are determined in the intermediate coupling scheme (values < 0.01 are not listed). The effective cross section Σ^{eff} is calculated by using Eqn. (2) in section III.

λ (μm)	Emission Transition (J→J')	$S^{ED}+S^{MD}$ [x$10^{-20}cm^2$]	Σ^{eff} [x10^{-18}cm]	ESA/ Bleaching / Reabsorption Transitions (J→J')	$S^{ED}+S^{MD}$ [x$10^{-20}cm^2$]	Σ^{eff} [x10^{-18}cm]
1.44				$^4F_{5/2}\rightarrow{}^4G_{9/2}$	1.07	2.55
1.48				$^2H_{9/2}\rightarrow{}^4G_{9/2}$	0.70+0.01	0.98
1.36	$^4F_{3/2}\rightarrow{}^4I_{13/2}$*	0.53	2.01	$^4I_{13/2}\rightarrow{}^4F_{3/2}$*	0.53	0.58
1.37				$^4I_{15/2}\rightarrow{}^4F_{7/2}$	3.03	2.83
1.35				$^4I_{15/2}\rightarrow{}^4S_{3/2}$	0.85	0.80
1.34				$^4F_{3/2}\rightarrow{}^2K_{13/2}$	0.02	0.07
1.335				$^4F_{3/2}\rightarrow{}^4G_{7/2}$*	0.59	2.25
1.255				$^4F_{3/2}\rightarrow{}^4G_{9/2}$*	0.82	3.89
1.19	$^4F_{5/2}\rightarrow{}^4I_{13/2}$*	2.71	7.78	$^4I_{13/2}\rightarrow{}^4F_{5/2}$*	2.71	3.34
1.17	$^2H_{9/2}\rightarrow{}^4I_{13/2}$*	0.37	0.65	$^4I_{13/2}\rightarrow{}^2H_{9/2}$*	0.37	0.46
1.21				$^2H_{9/2}\rightarrow{}^2K_{15/2}$[(a)]	5.49	9.33
1.18				$^4F_{5/2}\rightarrow{}^2K_{15/2}$	0.01	0.04
1.20				$^2H_{9/2}\rightarrow{}^2G_{9/2}$	0.38+0.04	0.73
1.17				$^4F_{5/2}\rightarrow{}^2G_{9/2}$	0.36	1.05
1.17				$^2H_{9/2}\rightarrow{}^2D_{3/2}$	0.48	0.85
1.15				$^4F_{5/2}\rightarrow{}^2D_{3/2}$	0.00+0.01	0.03
1.14				$^2H_{9/2}\rightarrow{}^4G_{11/2}$	0.08+0.01	0.17
1.12				$^4F_{5/2}\rightarrow{}^4G_{11/2}$[(a)]	1.08	3.30
1.07	$^4F_{3/2}\rightarrow{}^4I_{11/2}$*	2.11	10.09	$^4I_{11/2}\rightarrow{}^4F_{3/2}$*	2.11	3.37
1.07				$^4I_{13/2}\rightarrow{}^4F_{7/2}$	3.06	4.19
1.06				$^4I_{13/2}\rightarrow{}^4S_{3/2}$	0.85	1.17
1.02				$^4I_{15/2}\rightarrow{}^2H_{11/2}$	0.70	0.89
1.05				$^4F_{3/2}\rightarrow{}^2K_{15/2}$	0.03	0.12
1.045				$^4F_{3/2}\rightarrow{}^2G_{9/2}$	0.25	1.20
1.00				$^4F_{3/2}\rightarrow{}^4G_{11/2}$	0.27	1.38
0.97	$^4F_{5/2}\rightarrow{}^4I_{11/2}$*	1.66	5.88	$^4I_{11/2}\rightarrow{}^4F_{5/2}$*	1.66	2.94
0.95	$^2H_{9/2}\rightarrow{}^4I_{11/2}$*	0.07	0.16	$^4I_{11/2}\rightarrow{}^2H_{9/2}$*	0.07	0.13

0.94				$^4I_{13/2}\rightarrow{}^4F_{9/2}$	3.36	5.25
0.96				$^2H_{9/2}\rightarrow{}^2P_{1/2}$	0.82	1.75
0.94				$^4F_{5/2}\rightarrow{}^2P_{1/2}$	0.00	0.01
0.89	$^4F_{3/2}\rightarrow{}^4I_{9/2}$*	2.28	13.10	$^4I_{9/2}\rightarrow{}^4F_{3/2}$*	2.28	5.24
0.885				$^4I_{11/2}\rightarrow{}^4F_{7/2}$*	3.00	5.81
0.88				$^4I_{11/2}\rightarrow{}^4S_{3/2}$*	0.53	1.04
0.84				$^4I_{13/2}\rightarrow{}^2H_{11/2}$	0.17+0.01	0.31
0.91				$^2H_{9/2}\rightarrow{}^2D_{5/2}$	0.82	1.84
0.89				$^4F_{5/2}\rightarrow{}^2D_{5/2}$	0.00	0.02
0.86				$^4F_{3/2}\rightarrow{}^2P_{1/2}$	0.00	0.04
0.82	$^4F_{5/2}\rightarrow{}^4I_{9/2}$*	3.23	13.51	$^4I_{9/2}\rightarrow{}^4F_{5/2}$*	3.23	8.11
0.805	$^2H_{9/2}\rightarrow{}^4I_{9/2}$*	0.37+0.02	1.00	$^4I_{9/2}\rightarrow{}^2H_{9/2}$*	0.37+0.02	1.00
0.79				$^4I_{11/2}\rightarrow{}^4F_{9/2}$	1.26	2.73
0.78				$^4I_{15/2}\rightarrow{}^2K_{13/2}$	0.03	0.04
0.81				$^4F_{3/2}\rightarrow{}^2D_{5/2}$	0.01	0.03

[(a)]Not clear why these transitions are not observed.

*Indicated as the main observed transitions for Nd:RPB in Figure 5.

Table 2. Calculated radiative τ^{rad} and measured τ^{meas} lifetimes for the initial level J of the relevant emission, reabsorption, cross relaxation, and excited state absorption processes for Nd:KPB and Nd:RPB. For comparison lifetimes of Nd:KPC are given.

Energy J level	Nd:KPB τ^{rad}, (τ^{meas}) [ms]		Nd:RPB τ^{rad}, (τ^{meas}) [ms]		Nd:KPC τ^{rad}, (τ^{meas}) [ms]	
$^4I_{11/2}$	45.8, (5.0[e])		57.5		33.2[a], (2.0-2.3)[d]	
$^4I_{13/2}$	14.3 (1.1[e])		18.2		9.7[a], (6-0.3)[d]	
$^4I_{15/2}$	12.6 (0.7[e], 1.2[f])		16.2		8.3[a], (8-0.2)[d]	
$^4F_{3/2}$	0.128, (0.145)		0.116, (0.119)		0.111[a], (0.255)	
$^4F_{5/2}$	0.101	0.208[b], 0.153[c]	0.094	0.214[b], 0.150[c]	0.085[a]	0.175[b], 0.130[c]
$^2H_{9/2}$	0.574	(0.124)	0.894	(0.126)	0.480[a]	(0.002)

[a] determined by using Judd-Ofelt intensity parameters of Nd:KPC[17] Ω_2= 13.26, Ω_4= 5.63, Ω_6= 4.71 [x10^{-20} cm^2]

[b] τ^{rad} determined by assuming statistically distributed populations using the high temperature limit E_i<<kT.

[c] τ^{rad} determined by assuming statistically distributed populations using crystal field level energies of Nd:KPB.

[d] after Jenkins et al.[15]; variation of Nd concentration 0.88-7.4·10^{19} cm^{-3}.

[e] after Hoemmerich et al.[18], Nd concentration ~ 4.7·10^{19} cm^{-3}.

[f] measured by exciting the $^4I_{15/2}$ level and detecting at 2.5 μm; Nd concentration ~ 1.7-2.35·10^{19} cm^{-3}.

Table 3. Calculated line strengths S of induced electric dipole (ED) and of magnetic dipole (MD) transitions for Nd:KPB (a) and Nd:RPB (b). Cross relaxation (CR) depopulates the lower long lived laser levels ^4I_J (J=13/2 and 15/2). The integrated cross sections Σ^{eff} of Nd:KPB are slightly higher than for Nd:RPB.

	λ (μm)	Transition (J→J')	$S^{ED}+S^{MD}$ ($x10^{-20}cm^2$)	Σ^{eff} [$x10^{-18}$cm]
(a)				
CR1	5.07	$^4I_{13/2}\rightarrow{}^4I_{11/2}$	4.91+0.93	1.79
	5.31	$^4I_{9/2}\rightarrow{}^4I_{11/2}$	4.43+0.70	2.10
CR2	2.49	$^4I_{15/2}\rightarrow{}^4I_{11/2}$	1.31	0.72
	2.59	$^4I_{9/2}\rightarrow{}^4I_{13/2}$	1.44	1.22
CR3	4.88	$^4I_{15/2}\rightarrow{}^4I_{13/2}$	5.35+0.71	1.69
	5.07	$^4I_{11/2}\rightarrow{}^4I_{13/2}$	4.91+0.93	2.09
(b)				
CR1	5.07	$^4I_{13/2}\rightarrow{}^4I_{11/2}$	4.44+0.93	1.55
	5.31	$^4I_{9/2}\rightarrow{}^4I_{11/2}$	3.99+0.70	1.80
CR2	2.49	$^4I_{15/2}\rightarrow{}^4I_{11/2}$	1.17	0.61
	2.59	$^4I_{9/2}\rightarrow{}^4I_{13/2}$	1.29	1.02
CR3	4.88	$^4I_{15/2}\rightarrow{}^4I_{13/2}$	4.83+0.71	1.45
	5.07	$^4I_{11/2}\rightarrow{}^4I_{13/2}$	4.44+0.93	1.80

Figure 1

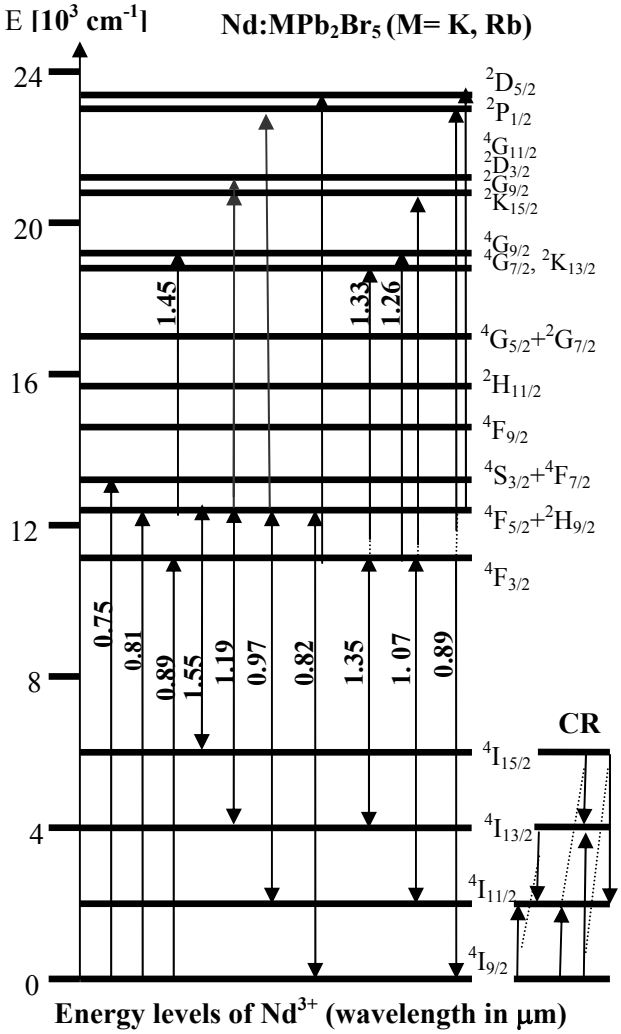

Fig. 1. Energy level diagram of Nd:MPB (M= K, Rb) displays new laser transitions from the $^4F_{5/2}$+ $^2H_{9/2}$ level at 1.18 and 0.97 μm and potential transitions at 0.82 and 1.55 μm, in addition to the conventional laser transitions at 1.07 and 1.35 μm from the $^4F_{3/2}$ level. Excited state absorption transitions resulting from the $^4F_{5/2}$+ $^2H_{9/2}$ and $^4F_{3/2}$ levels as well as depopulation mechansims for the long lived lower laser levels ^4I_J (J=13/2, 15/2) via cross relaxation (CR) are indicated. The pump bands at 0.75, 0.81, and 0.89 μm are indicated. (Transitions resulting from the $^4F_{7/2}$+ $^4S_{3/2}$ level have been neglected in order to simplify the discussion.)

Figure 2

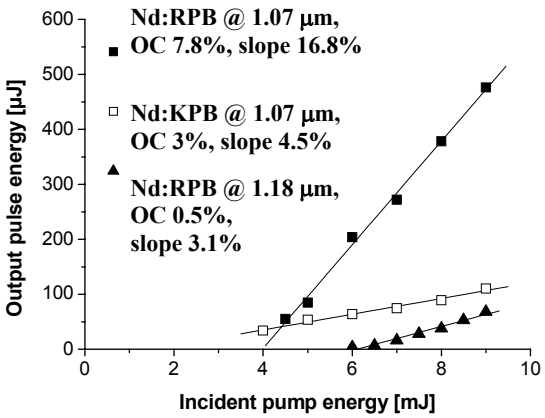

Fig. 2. Input-output characteristic for an OPO-pumped Nd:KPB crystal lasing at 1.07 μm and Nd:RPB crystal lasing at 1.07 μm and 1.18 μm (taken from Ref. 1). The slope efficiency is given for output pulse energy with respect to absorbed pump energy. In order to achieve lasing at 1.07 μm the $^4F_{3/2}$ level was directly pumped, while for the laser wavelength 1.18 μm and 0.97 μm the $^4F_{5/2}$ level was pumped.

Figure 3

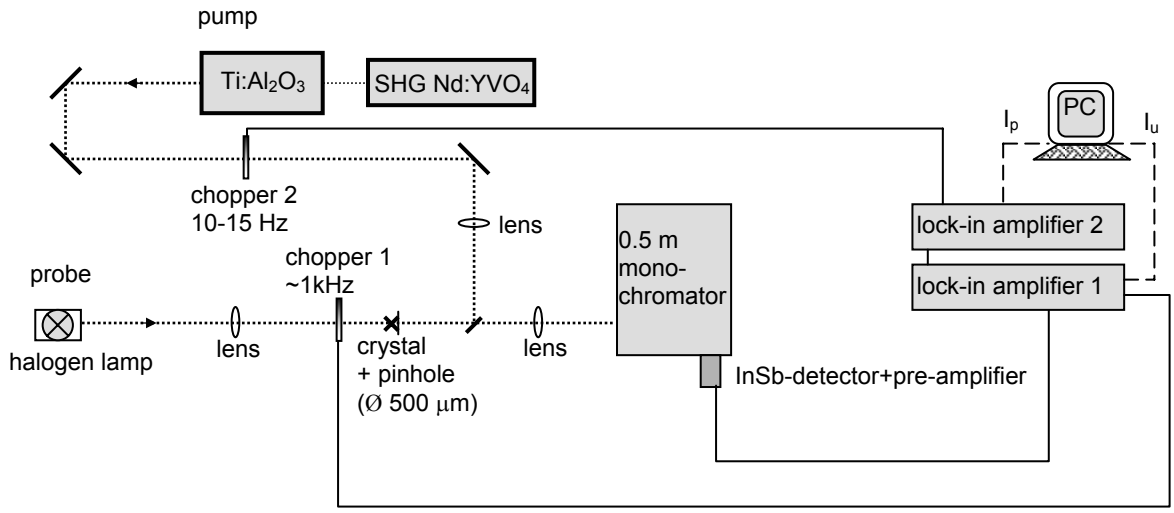

Fig. 3. Experimental setup of the cw pump-probe technique.

Figure 4

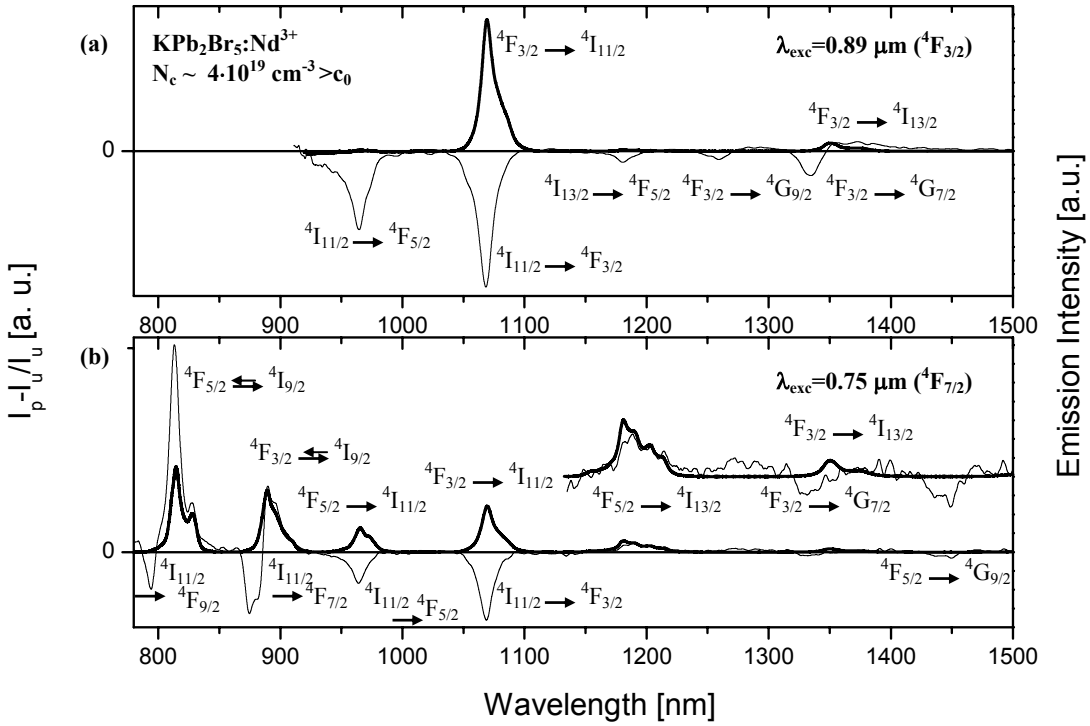

Fig. 4. Emission spectra (thick line) and pump-probe spectra (thin line) of Nd^{3+}:KPb_2Br_5 determined by pumping into either the $^4F_{3/2}$ (a) or $^4F_{7/2}$+$^4S_{3/2}$ (b) level, respectively (using same crystal for both spectra). The inset in (b) displays a ~ 5x magnification for the wavelength range 1135 – 1500 nm. Reabsorption and excited state absorption compete with gain as indicated. Depopulation via cross relaxation leads to less reabsorption of transitions from the $^4I_{13/2}$ level compared to the $^4I_{11/2}$. Note that only the main transitions are indicated (Table 1 shows others) and that the $^4F_{5/2}$+$^2H_{9/2}$ and $^4F_{7/2}$+$^4S_{3/2}$ levels are abbreviated by $^4F_{5/2}$ and $^4F_{7/2}$, respectively.

Figure 5

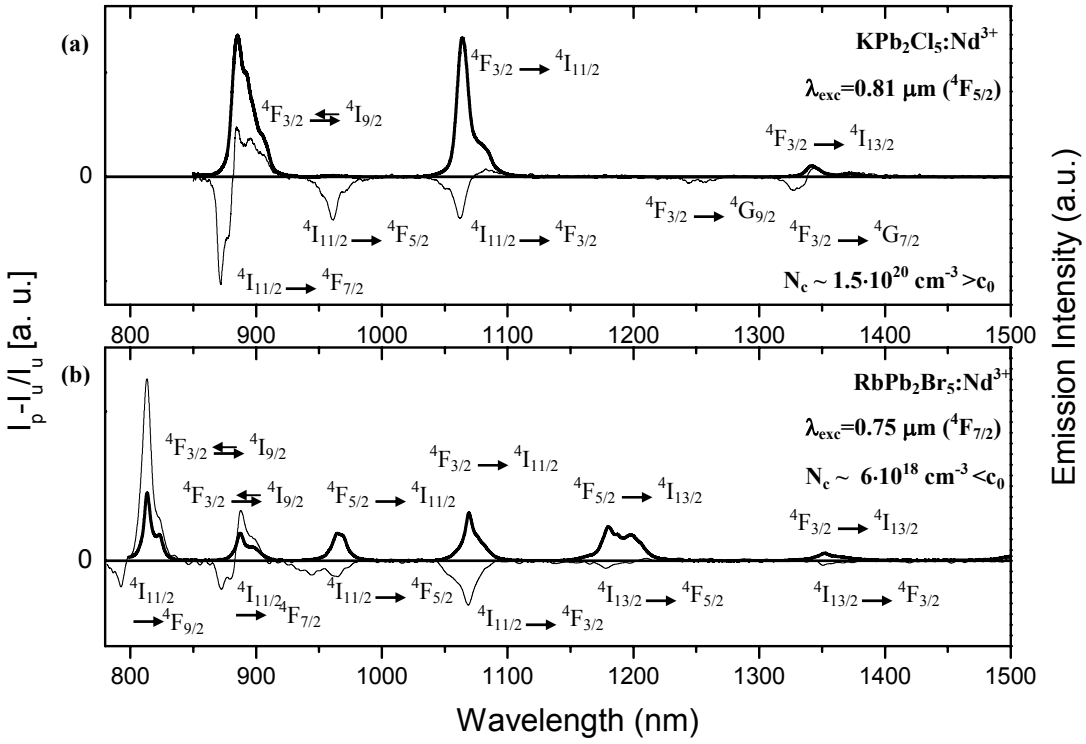

Fig. 5. Emission spectra (thick line) and pump-probe spectra (thin line) of Nd^{3+}:KPb_2Cl_5 determined by pumping into the $^4F_{5/2}$+$^2H_{9/2}$ level (a) and Nd^{3+}:$RbPb_2Br_5$ determined by pumping into the $^4F_{7/2}$+$^4S_{3/2}$ level (b). Reabsorption and excited state absorption compete with gain as indicated. Depopulation via cross relaxation leads to less reabsorption of transitions from the $^4I_{13/2}$ level compared to the $^4I_{11/2}$ in the case of Nd:KPC compared to Nd:RPB, due to the higher Nd concentration. (Note that the emission of Nd:RPB is not blackbody corrected.) The feature near 0.94 μm (b) could be due to the $^4I_{13/2}\rightarrow{}^4F_{9/2}$ transition. Note that only the main transitions are indicated (Table 1 shows others) and that the $^4F_{5/2}$+$^2H_{9/2}$ and $^4F_{7/2}$+$^4S_{3/2}$ levels are abbreviated by $^4F_{5/2}$ and $^4F_{7/2}$, respectively.